Structures 34 (2021) 4142–4157

Contents lists available at ScienceDirect

Structures

journal homepage: www.elsevier.com/locate/structures

Probabilistic seismic assessment of steel gabled frames with web-tapered members under near-fault ground motions along strike-normal and strike-parallel components

Mohammad Malekizadeh [a,*], Nader Fanaie [b,*], Ali Akbar Pirasteh [c]

[a] Department of Civil Engineering, Academic Center for Education, Culture and Research, Khuzestan Branch, Ahvaz, Iran
[b] Department of Civil Engineering, K. N. Toosi University of Technology, Tehran, Iran
[c] Department of Civil Engineering, Faculty of Engineering, Shahid Chamran University of Ahvaz, Ahvaz, Iran

ARTICLE INFO

Keywords:
Steel gabled frames
Strike-normal
Strike-parallel
Incremental dynamic analysis
Probabilistic seismic demand model
Mean annual frequency

ABSTRACT

The seismic assessment of steel gabled frames (SGFs) is of great importance and a key problem in any high-seismicity region, given the enormous costs of industrial equipment and the remarkable number of individuals working in such structures. Near-fault ground motions, especially their strike-normal component that usually contain a long-period pulse in the velocity time-history, can lead to a significant demand in these structures in comparison to the far-fault ground motions. Although numerous studies have confirmed the destructive effects of near-fault ground motions on concrete and steel structures, no research has been devoted to the impact of this ground motions on steel gabled structures yet. Hence, the findings of this research can unveil novel dimensions of such structures. In this regard, in the present paper, an incremental dynamic analysis (IDA) was conducted for the first time on four SGFs with the spans of 20 m and 60 m and heights of 6 m and 12 m using far-fault ground motions (OR set), as well as near-fault ground motions along the strike-normal and strike-parallel components (SN and SP sets, respectively). The results were presented in the form of multi-record IDA curves, summarized IDA curves, probabilistic seismic demand models (PSDMs) and probabilistic seismic demand analysis (PSDA) curves. The outcomes indicated that compared to far-fault ground motions, near-fault ground motions (especially pulse-like ones) produced significant changes on the seismic behavior of long-period SGFs, resulting in raises the changes of stiffness and demand sensitivity, reduces the dynamic capacity, enhances the data dispersion and uncertainty, and increases the mean annual frequencies (MAFs) in such structures. However, the results of PSDA analysis showed that under any type of ground motion (OR, SN and SP), short-period SGFs are more vulnerable than long-period SGFs and should be prioritized for retrofitting. Finally, the importance of combining the hazard curve of the study region with the results of IDA analysis of the structure in evaluating the seismic behavior of SGFs is highlighted.

1. Introduction

Nowadays, with the advances of construction techniques, building materials, and design theory, steel gabled frame (SGF) systems have been widely accepted in developed countries with numerous applications, given their special advantages, such as the creation of long spans without middle columns (clear span), the proper performance of the structure in most cases due to the symmetry, fast installation and easy transfer to other spaces due to the connections with nuts and bolts, and low weight despite large dimensions. Instances of such structures are aircraft hangars, industrial factories, warehouses, sports complexes, conference halls, pools, etc. SGFs are constructed in single-, two-, and multi-span forms, among which the single-span ones are more common and enjoy greater applicability due to their specific advantages, such as providing a space for the passage of enormous vehicles such as aircrafts, creating structures with unique architecture, and having proper structural style. In seismic design, SGF systems are usually designed as an ordinary moment frame (OMF) due to their low ductility capacity. In SGFs, in order to bring an optimal design in steel material consumption, they usually have a variable web height along the entire length of the columns as well as part of the length of the rafters, which the rate of change of web height in SGFs members depends on the distribution of

* Corresponding authors.
E-mail addresses: mohammadmalekizadeh@yahoo.com (M. Malekizadeh), fanaie@kntu.ac.ir (N. Fanaie), pirasteh@scu.ac.ir (A.A. Pirasteh).

https://doi.org/10.1016/j.istruc.2021.10.007
Received 1 August 2021; Received in revised form 1 October 2021; Accepted 4 October 2021

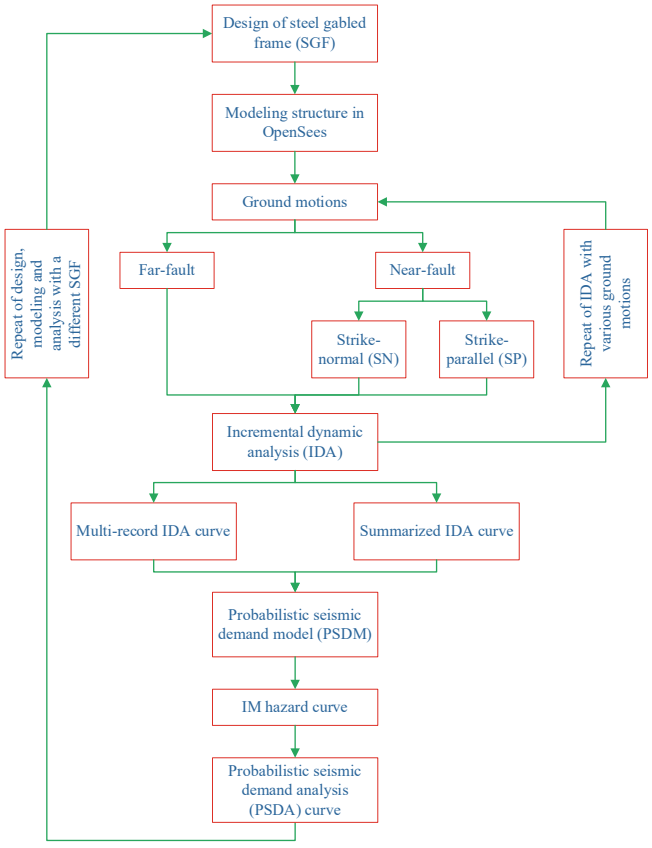

Fig. 1. General flowchart of the present study.

strong-axis bending moments along their members. In SGFs, the strong-axis bending moments in the shoulder part and partially in the ridge part is more than the middle part of the rafter. Therefore, the critical part length in SGF rafters is mainly considered span/10 from the eave line, but in the ridge part, in order to prevent the occurrence of strong inertial forces, usually the web height is not increased and it is design as a prismatic. Also, because of the special geometry of SGFs, their column bases are generally considered as a hinge support, which prevents the bending moment from being transferred to the foundation. This makes the foundation of SGFs lighter and therefore more economical.

The seismic assessment of SGFs is of great importance and a key problem in any high-seismicity region (such as Tehran), given the enormous costs of industrial equipment and the remarkable number of individuals working in such structures. Near-fault ground motions, especially their strike-normal component that usually contain a long-period pulse in the velocity time-history, can lead to a significant demand in these structures in comparison to the far-fault ground motions. Also, with respect to the dramatic development of SGFs construction in developed countries, many of them are likely in vicinity of the faults and will experience near-fault ground motions in the future. This can significantly increase the importance of seismic assessment of SGFs against such ground motions.

The 1966 Parkfield earthquake, the 1979 Imperial Valley earthquake, the 1994 Northridge earthquake, the 1999 Chi-Chi earthquake and the 2008 Wenchuan earthquake revealed unique characteristics of ground motions in near-fault regions [1–3]. These near-source outcomes cause most of the seismic energy from the rupture is released in a single coherent long-period pulse at the beginning of the ground motion [4]. The radiation pattern of the shear dislocation on the fault causes this pulse of motion to be oriented in the direction perpendicular to the fault, it causes the strike-normal component to be stronger than its strike-parallel counterpart in near-fault ground motions [5–7]. The pulses are strongly influenced by the rupture mechanism, including the slip direction relative to the site and the location of the recording station relative to the fault. It is termed as forward-directivity effect due to the propagation of the rupture toward the recording site [1,8]. Pulse-like ground motions are caused mainly by the forward-directivity effect, which are observed at a site when the fault rupture propagates toward the site with a velocity close to shear wave velocity [9,10]. Nevertheless, it should be noted that not all pulse-like ground motions are the result of

Table 1
Section dimensions of the rafter and column members.

Components	Model 1 (m)	Model 2 (m)	Model 3 (m)	Model 4 (m)
Column web height at top	0.8	1	1.5	1.5
Column web height at bottom	0.3	0.3	0.3	0.3
Rafter web height at ridge	0.4	0.5	1	1
Rafter web height at eave	0.8	1	1.5	1.5
Web thickness	0.008	0.01	0.014	0.014
Flange thickness	0.01	0.012	0.018	0.02
Flange width	0.18	0.24	0.34	0.4

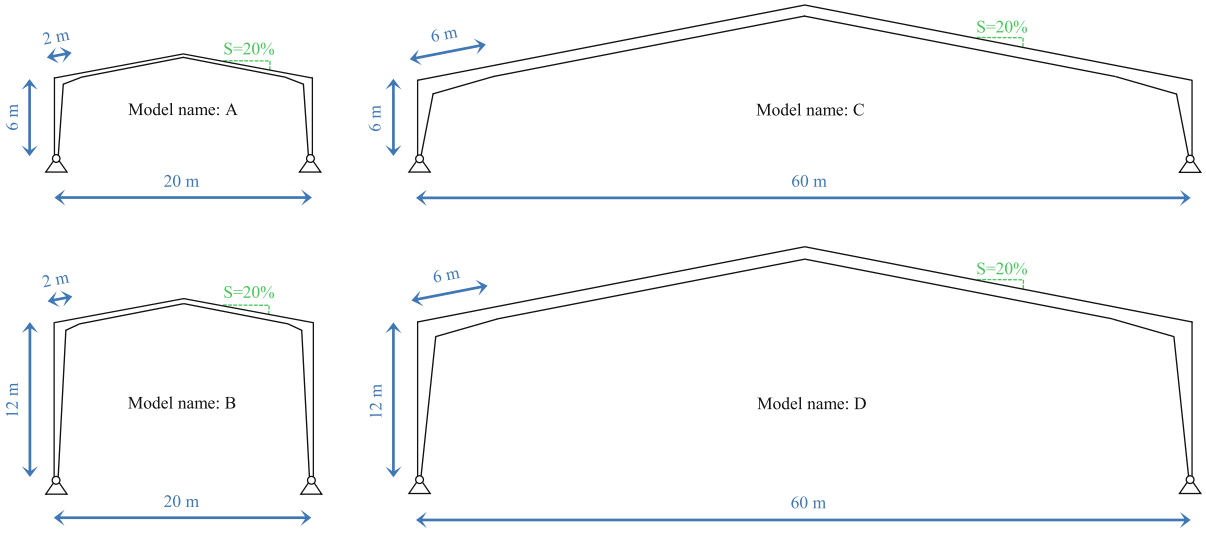

Fig. 2. Geometrical dimensions of the studied SGFs.

Table 2
Specifications of prismatic microelements.

	Model 1		Model 2		Model 3		Model 4	
	Column	Rafter	Column	Rafter	Column	Rafter	Column	Rafter
Δh_0 (m)	0.02	0.02	0.02	0.02	0.02	0.02	0.02	0.02
l_0 (m)	0.24	0.10	0.34	0.08	0.10	0.24	0.20	0.24
n_0	2 × 25	2 × 33	2 × 35	2 × 66	2 × 60	2 × 66	2 × 60	2 × 66

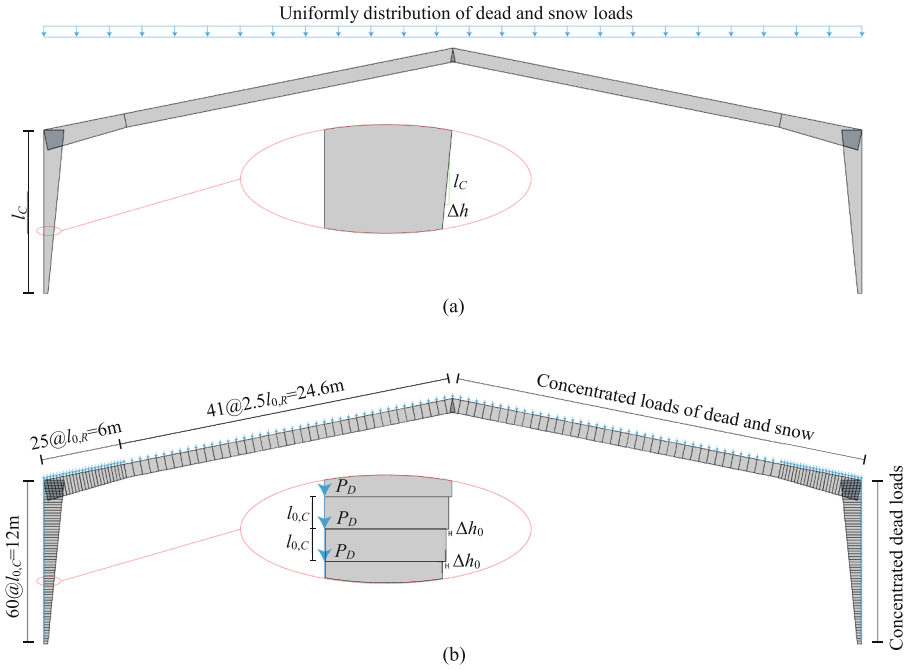

Fig. 3. Schematic representation of Model 4: (a) initial model, (b) final model developed in OpenSees.

Table 3
Fundamental period of the studied SGFs.

No.	OpenSees (sec)	SAP2000 (sec)	Error (%)
1	0.90	0.89	1
2	1.53	1.51	1
3	0.63	0.62	1
4	1.31	1.30	1

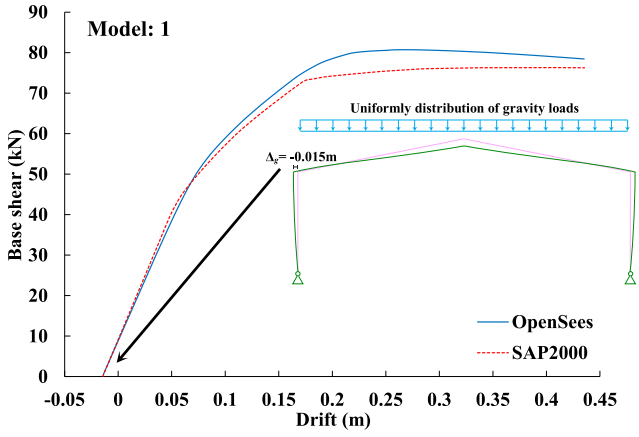

Fig. 4. Pushover curve for model 1.

forward-directivity effects and the appearance of pulses is likely caused by effects other than forward-directivity, such as basins effects, surface wave effects or surficial soil effects [11–14].

The long-period velocity pulses in near-fault ground motions lead to nonlinear deformations and severe damages to engineering structures. This problem has attracted the attention of many researchers in earthquake engineering community [15–19]. Recent studies on dams revealed that near-fault pulse-like ground motions resulted in large horizontal displacements [20,21], high principal stresses [22,23], and considerable residual deformations in the crests [24]. According to reports, in conventional buildings, near-fault pulse-like ground motions led to large demands in the lower half of structures [25,26], remarkable damages to foundation connections [27], and even the collapse [28]. Moreover, the destructive and unfavorable effects of near-fault pulse-like ground motions on the base-isolated buildings were evaluated [29–31]. Some recent research on intake towers demonstrated great nodal displacements, large curvatures at the lower part of structures [32], and serious damages [33] caused by near-fault pulse-like ground motions. Furthermore, it has been reported that such motions produced greater displacements and internal forces in the bridges compared to the non-pulse ground motions [34–36]. In near-fault ground motions, where the strike-normal component usually contain a long-period pulse in the velocity time-history, it is expected to cause more damages to structures compared to the strike-parallel component. However, some studies showed that the strike-parallel component might result in more damages to structures [37,38]. Therefore, in SGFs, which have different dynamic properties from those of conventional buildings, the strike-parallel component of a fault may result in a different response and create greater demand in the structure compared to its strike-normal

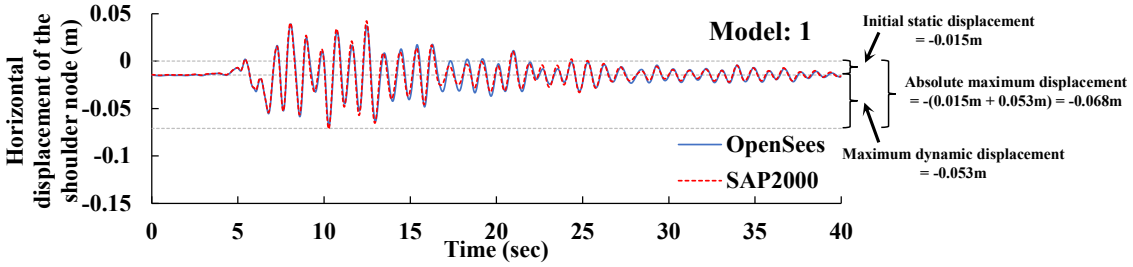

Fig. 5. Horizontal displacement time-history curve corresponding to the shoulder node for model 1.

Table 4
Far-fault ground motions [64].

No.	Event	Station	M_w	R_{rup} (km)	PGA (g)	PGV (cm/sec)	$D_{5\text{-}95\%}$ (sec)
1	Borrego Mountain	El Centro Array #9	6.80	46.00	0.057	13.2	28.7
2	Loma Prieta	APEEL 2E Hayward Muir Sch	6.90	57.40	0.171	13.7	12.8
3	Loma Prieta	Fremont-Emerson Court	6.90	43.40	0.141	12.9	17.9
4	Loma Prieta	Halls Valley	6.90	31.60	0.134	15.4	16.2
5	Loma Prieta	Salinas-John & Work	6.90	32.60	0.112	15.7	20.3
6	Loma Prieta	Palo Alto-SLAC Lab.	6.90	36.30	0.194	37.5	12.5
7	Northridge	Covina-W Badillo	6.70	56.10	0.100	5.8	17.4
8	Northridge	Compton-Castlegate St.	6.70	49.60	0.136	7.1	23.4
9	Northridge	LA-Centinela St.	6.70	30.90	0.322	22.9	12.4
10	Northridge	Lakewood-Del Amo Blvd.	6.70	59.30	0.137	11.2	20.8
11	Northridge	Downey-Co. Maint. Bldg.	6.70	47.60	0.158	13.8	17.3
12	Northridge	Bell Gardens-Jaboneria	6.70	46.60	0.068	7.6	20.1
13	Northridge	Lake Hughes #1	6.70	36.30	0.087	9.4	13.9
14	Northridge	Lawndale-Osage Ave.	6.70	42.40	0.152	8.0	23.3
15	Northridge	Leona Valley #2	6.70	37.70	0.063	7.2	12.5
16	Northridge	Palmdale-Hwy 14 & Palmdale	6.70	43.60	0.067	6.9	18.2
17	Northridge	LA-Pico & Sentous	6.70	32.70	0.186	14.3	14.8
18	Northridge	West Covina-S. Orange Ave.	6.70	54.10	0.063	5.9	19.3
19	Northridge	Terminal Island-S. Seaside	6.70	60.00	0.194	12.1	13.4
20	Northridge	LA-E Vernon Ave.	6.70	39.30	0.153	10.1	15.9

counterpart.

The design basis for web-tapered members was established based on Lee et al. [39–42] and further extended by Forest and Murray [43], Shiomi and Kurata [44] and Ashakul and Murray [45]. Moreover, experimental investigations on the seismic behavior of gabled frames with web-tapered members have been conducted by Hwang et al. [46], Hong and Uang [47] and Su et al. [48]. However, because of the complexity of design and modeling as well as the low ductility of SGFs with web-tapered members, very limited analytical research is available for their seismic behavior. Due to the fact that such structures are very sensitive to the formation of plastic hinges, it is essential to evaluate their behavior in the nonlinear region and it seems that the use of incremental dynamic analysis (IDA), which consists of a large number of nonlinear time-history analyses under a set of ground motions, is a suitable option for them. On the other hand, ground motions and their effects on structures are essentially probabilistic. Accordingly, it is better to use probabilistic methods to estimate the expected demands of structures under future ground motions. In this regard, performance-based earthquake engineering (PBEE) is a well-known and valid method for considering probabilistic parameters in seismic assessment of new and existing structures [49]. For this purpose, PBEE uses the probabilistic seismic demand analysis (PSDA) to obtain the mean annual frequency (MAF) of exceeding a specified demand for a given structure at a designated site. Briefly, PSDA combines a ground motion (e.g., spectral acceleration) hazard curve for the designated site, typically computed through probabilistic seismic hazard analysis (PSHA), with the demand (e.g., drift angle) results from nonlinear dynamic analysis of the given structure under a set of ground motions. Also, different sources of uncertainty can be considered in this analysis (e.g., record to record uncertainty, etc.) [50–52].

Although a review of the literature corroborates the destructive effects of near-fault ground motions on the above-mentioned structures, there is no study dealing with such effects on steel gabled structures and the present study is hoped to offer a new perspective to the research in this field. To this aim, four SGFs with the spans of 20 m and 60 m and heights of 6 m and 12 m undergo IDA analysis in this study for the first time using far-fault ground motions (set OR), as well as near-fault ground motions along the strike-normal and strike-parallel components (SN and SP sets, respectively). The results will be presented in the form of multi-record IDA curves, summarized IDA curves, Probabilistic seismic demand models (PSDMs), and PSDA curves. A general flowchart for the present research is given in Fig. 1.

2. Geometrical specifications of the studied SGFs

In the present paper, four 2D SGF models are utilized with different spans and heights to analyze and investigate the effect of near-fault ground motions. The names of the models as well as their geometrical dimensions are given in Fig. 2. As can be seen, the entire length of the columns and the region with a length of span/10 in rafters from the eave line are characterized by web-tapered members, while the rest of the length of the rafters up to the ridge is prismatic. The roof slope is considered to be 20% and the base of the columns enjoys hinge support. The fundamental period of SGFs is considered as a criterion for classification of models, so that models 1 and 3 as well as models 2 and 4 are classified as representative of short period SGFs and long period SGFs in this study, respectively.

The used steel was of ST37 type with the elasticity modulus of 2.039E + 10 kgf/m^2. In all of the studied SGFs, ordinary moment frame

Table 5
Near-fault pulse-like ground motions [65].

No.	Event	Station	M_w	R_{rup} (km)	V_{S30} (m/sec)	PGV (cm/s)	T_p (sec)
1	Imperial Valley-06	EC County Center FF	6.53	7.31	192.1	54.5	4.515
2	Imperial Valley-06	EC Meloland Overpass FF	6.53	0.07	186.2	50.2	3.346
3	Imperial Valley-06	El Centro Array #4	6.53	7.05	208.9	71.7	4.613
4	Imperial Valley-06	El Centro Array #5	6.53	3.95	205.6	91.5	4.046
5	Imperial Valley-06	El Centro Array #6	6.53	1.35	203.2	91.8	3.836
6	Imperial Valley-06	El Centro Array #7	6.53	0.56	210.5	69.6	4.228
7	Imperial Valley-06	El Centro Array #8	6.53	3.86	206.1	48.6	5.390
8	Imperial Valley-06	El Centro Differential Array	6.53	5.09	202.3	59.6	5.859
9	Landers	Yermo Fire Station	7.28	23.62	353.6	56.6	7.504
10	Northridge-01	Jensen Filter Plant	6.69	5.43	373.1	67.4	3.528
11	Northridge-01	Newhall-Fire Sta	6.69	5.92	269.1	120.3	1.036
12	Northridge-01	Newhall-W Pico Canyon Rd.	6.69	5.48	285.9	82.9	2.408
13	Northridge-01	Rinaldi Receiving Sta	6.69	6.50	282.3	167.2	1.232
14	Northridge-01	Sylmar-Converter Sta	6.69	5.35	251.2	130.3	3.479
15	Northridge-01	Sylmar-Converter Sta East	6.69	5.19	370.5	113.6	3.528
16	Kobe, Japan	KJMA	6.90	0.96	312.0	89.1	0.952
17	Kobe, Japan	Takarazuka	6.90	0.27	312.0	72.6	1.428
18	Chi-Chi, Taiwan	CHY101	7.62	9.96	258.9	52.9	4.599
19	Chi-Chi, Taiwan	TCU101	7.62	2.13	272.6	43.8	10.038
20	Chi-Chi, Taiwan	WGK	7.62	9.96	258.9	49.3	4.396

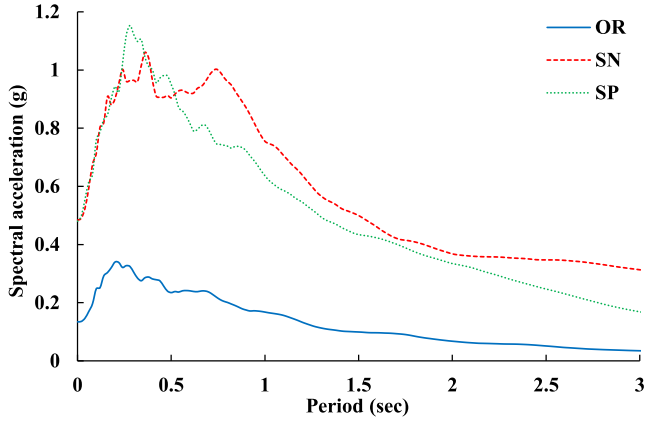

Fig. 6. Average of the elastic response spectra (5% damping) for the OR, SN and SP ground motions.

was incorporated as the lateral force resisting system. The location for modelling was assumed to be Tehran, Iran, a high-seismicity region and with tectonic characteristics of Class D soil according to NEHRP [53]. The gravity loads applied to the studied SGFs were dead load, balanced snow load, and unbalanced snow load. Walls and roofs were covered with sandwich panels with a weight of 360 kgf/m. ASCE/SEI 7-10 code [54] was used for gravity and lateral loading. The models were designed based on the load and resistance factor design (LRFD) method in line with AISC 360-10 and AISC 341-10 codes [55,56]. In designing 2D models, it is assumed that the distances between the fly braces in the rafter and the column are 1.7 m and 2 m, and the distances between the struts are 5.1 m and 3 m. According to AISC 341-10 code, as an OMF, there is no need to satisfy the stringent seismic compactness requirements. However, if non-compact or slender sections are used in SGFs, plastic hinges are unlikely to be expand due to the loosened local and lateral-torsional buckling requirements. Hence, in this study, the compact section according to AISC 360-10 code has been used. This causes more plastic moment capacity of the members to be used before being subjected to local and lateral-torsional buckling. Upon the end of the designing process and by employing the trial-and-error approach to achieve an economical model, the section dimensions of the rafter and column members were identified, which are given in Table 1.

3. Nonlinear modeling

For nonlinear modeling and analyzing the structural system, the OpenSees software [57], an open-source software utilized in the simulation of the seismic response of structural and geotechnical systems, was employed. The software seems promising as an important means of modeling and analyzing both the linear or nonlinear behaviors of structural systems.

OpenSees was employed in 2D modeling of the structures. The damping ratio was set to 5% and for modeling the viscous damping, Rayleigh damping was adopted [58]. In order to transfer the stiffness and resisting force of the rafter elements from the basic system to the global-coordinate system in a totally accurate way through geometric transformation, corotational transformation was applied. The nonlinear behavior of the materials in the rafters and columns was modeled using nonlinear beam-column element with distributed plasticity. for this purpose, in the OpenSees materials library, uniaxial bilinear steel material with kinematic hardening of 0.02 entitled steel01 was selected. Fiber section was assigned to the rafter and column elements. Hence, using defined nonlinear materials enables nonlinearization of all the components of such sections. It is noteworthy that in the present research, shear deformations are also accounted.

In modelling the web-tapered elements of the rafters and columns, prismatic microelements with different heights were employed and six integration points were considered for each microelement. Modeling of web-tapered members using prismatic microelements with variable height has been adopted in the study of Watwood [59], which confirms the use of this modeling method. Nevertheless, for the first time a model of SGFs with web-tapered members has been developed using prismatic microelements with variable height on the OpenSees platform. The study of Liu et al. [60] showed that in modeling web-tapered members using prismatic microelements with variable height, the accuracy of modeling increases with increasing the number of microelements. Hence, in order to increase the accuracy of modeling in the mentioned method, the height difference between the two sections of adjacent microelements (Δh_0) was considered to be a very small value, i.e., 0.02 m, and according to that, the length and number of microelements (l_0 and n_0, respectively) were determined for each member, which are presented in Table 2. It should be noted that in the prismatic area of the rafters, microelements with a length of $2.5\Delta l_{0,R}$ were used. Also, dead loads on the roofs and walls (i.e., rafters and columns) and snow loads only on the roofs (i.e., rafters) were applied concentratedly to each node according to the loading area. Because of the presence of sufficient lateral and lateral-torsional braces as well as the use of the compact

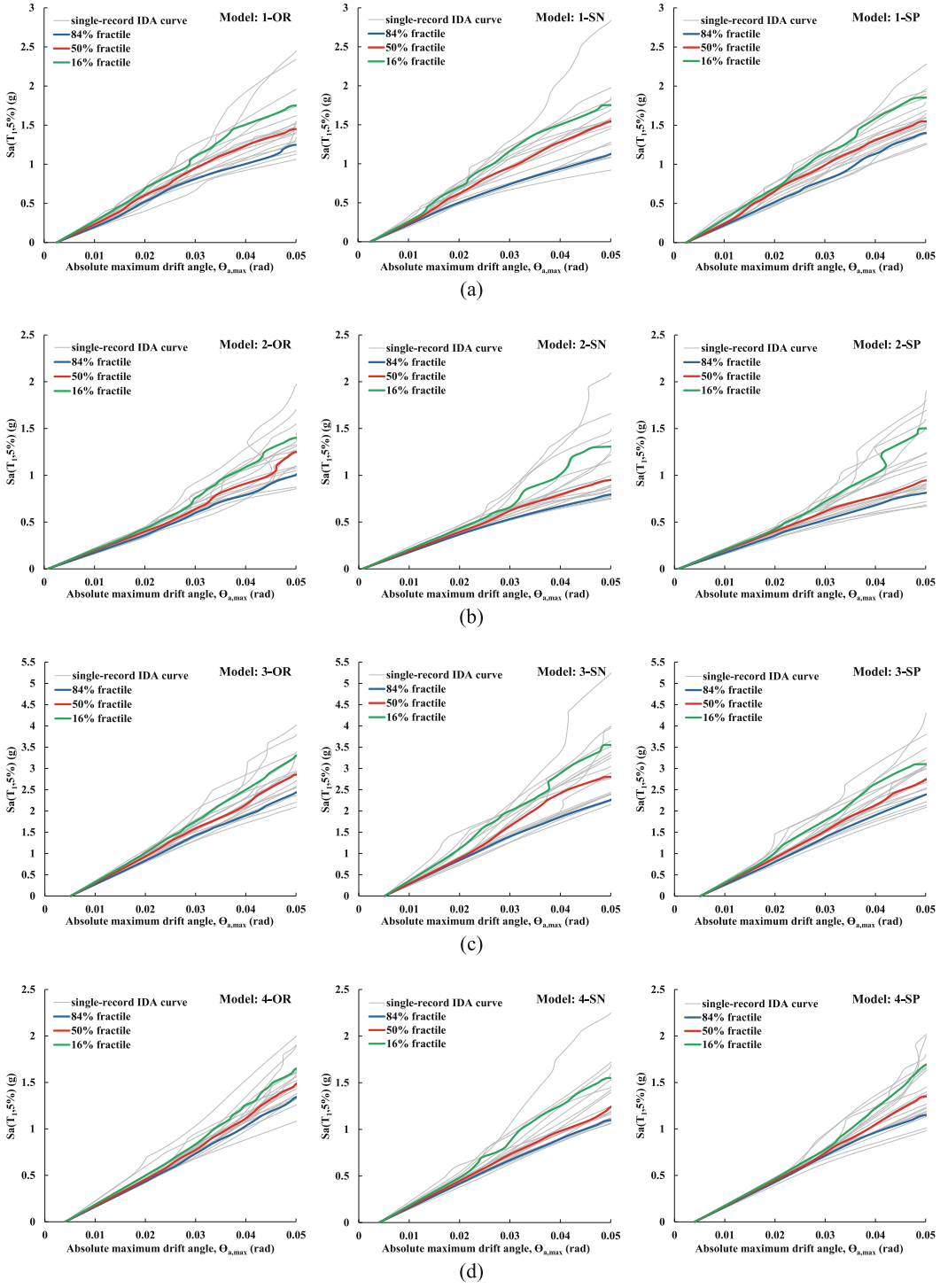

Fig. 7. Multi-record IDA curves and summarized IDA curves (16%, 50% and 84% fractiles) for (a) model 1, (b) model 2, (c) model 3, (d) model 4.

section in the members of the studied models, buckling is not expected to occur in the third dimension. As a result, the 2D models developed in OpenSees do not need to modeling these braces. For a better understanding, the schematic view of Model 4 with web-tapered elements and uniformly distribution of gravity loads (initial model) as well as with prismatic microelements and concentrated gravity loads (final model) is shown in Fig. 3.

4. Validation of the studied SGFs

As mentioned in the review of the literature, this study presents an in-depth evaluation of the seismic behavior of SGFs for the first time. Hence, since there was no comparison reference for the developed nonlinear model in the OpenSees software, it was compared in three steps by modal, pushover, and nonlinear time-history analyses with SAP2000 software [61]. Accordingly, it was necessary to identify the characteristics of the materials, sections, and nonlinear elements for the models developed in SAP2000 in accordance with those in the OpenSees. The results obtained by both pieces of software were compared for the mentioned three types of analysis and are presented in the following sections.

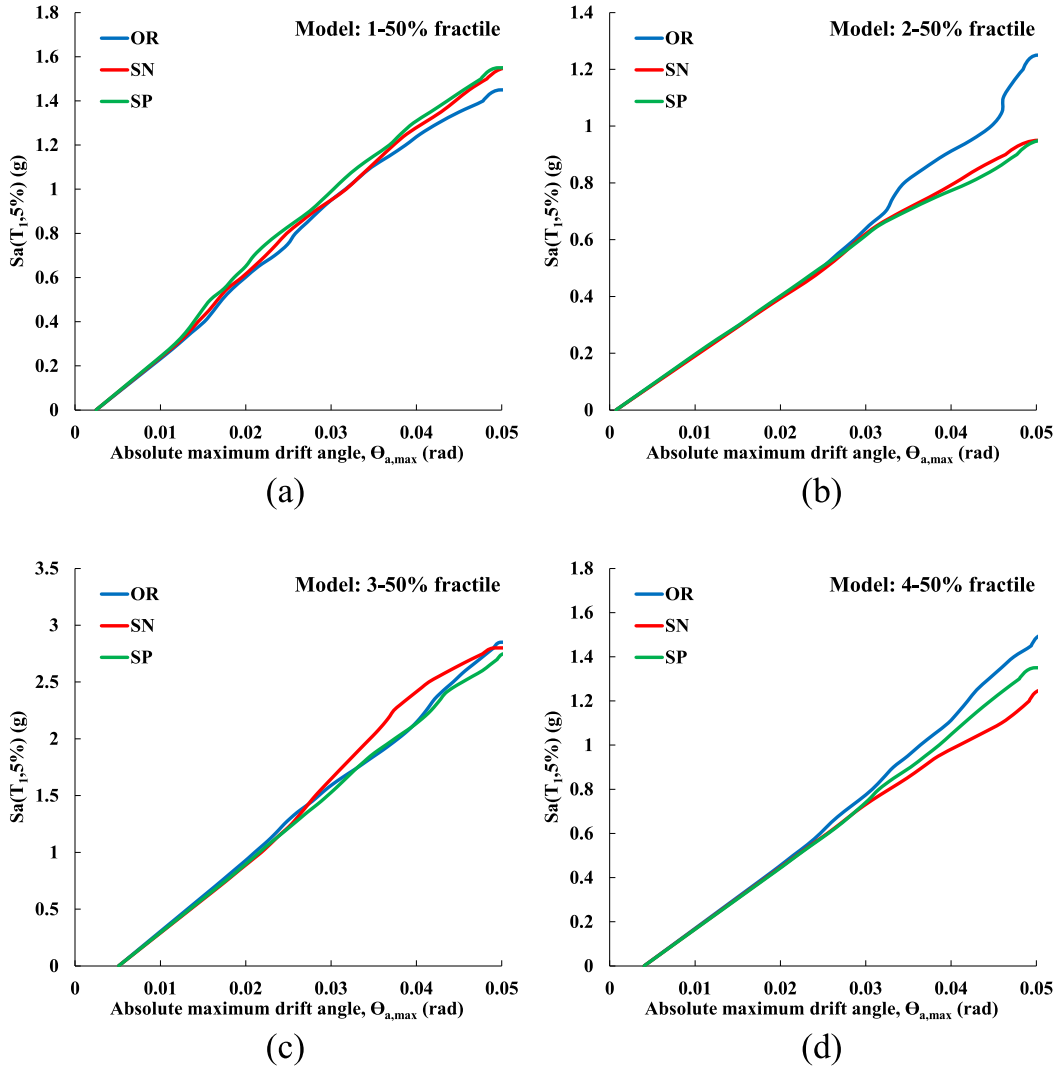

Fig. 8. Comparison of 50% fractile of the IDA curves for (a) model 1, (b) model 2, (c) model 3, (d) model 4.

4.1. Modal analysis

Validation of models by the modal analysis was gone through with the aim of comparing the dynamic properties such as first-mode period (fundamental period) of the structure in the OpenSees and SAP2000 software. The fundamental periods of the studied SGFs in the modal analysis by the mentioned software are represented in Table 3.

As observed in Table 3, the percentage of error between the fundamental periods in both pieces of software is negligible, proving the accurate modelling of SGFs in the linear region.

4.2. Pushover analysis

The aim of the nonlinear static (pushover) analysis was the comparison of the nonlinear behaviors of the structure in the OpenSees and SAP2000 software. Fig. 4 illustrates diagrams for the drift to the base shear (pushover curves) derived from the pushover analysis for Model 1 as a sample in both pieces of software. Prior to conducting any static or dynamic analysis under earthquake load, it is required to carry out the static analysis under gravity loads. Also, due to the greater criticality of balanced snow load than its unbalanced counterpart, the balanced snow load was used in conjunction with dead load in the gravity analysis. Of note, the target drift was identified with the help of FEMA 356 [62].

According to the pushover curves of Fig. 4, there is a slight difference in the linear region, which indicates accurate modeling of the linear region in both pieces of software, supporting the validation results of the modal analysis for this region. Furthermore, almost similar behaviors are also observed in the nonlinear region, indicating the acceptability of the results. As mentioned in the literature, SGFs do not have significant ductility due to their low degree of indeterminacy, and with the formation a small number of plastic hinges, instability occurs in this type of structures, as can be clearly seen in Fig. 4. Of note, due to the specific geometrical characteristics of SGFs (sloping beams), gravity loads create an initial negative drift in the shoulder. In addition, the hinge supports amplifies the mentioned negative drift, as can be clearly seen in Fig. 4.

4.3. Nonlinear time-history analysis

Validating the models through nonlinear time-history analysis was carried out with the aim of comparing the dynamic properties as well as the nonlinear behaviors of the structure in SAP2000 and OpenSees software. In Fig. 5, results for the nonlinear time-history analysis for Model 1 by using the Imperial Valley-06 earthquake record from the EC County Center FF station along strike-normal component with a peak ground acceleration (PGA) of 0.18 g are provided in the form of horizontal displacement time-history curves corresponding to the shoulder node using both pieces of software. Since the analysis presented in the present paper consists of a large number of nonlinear time-history

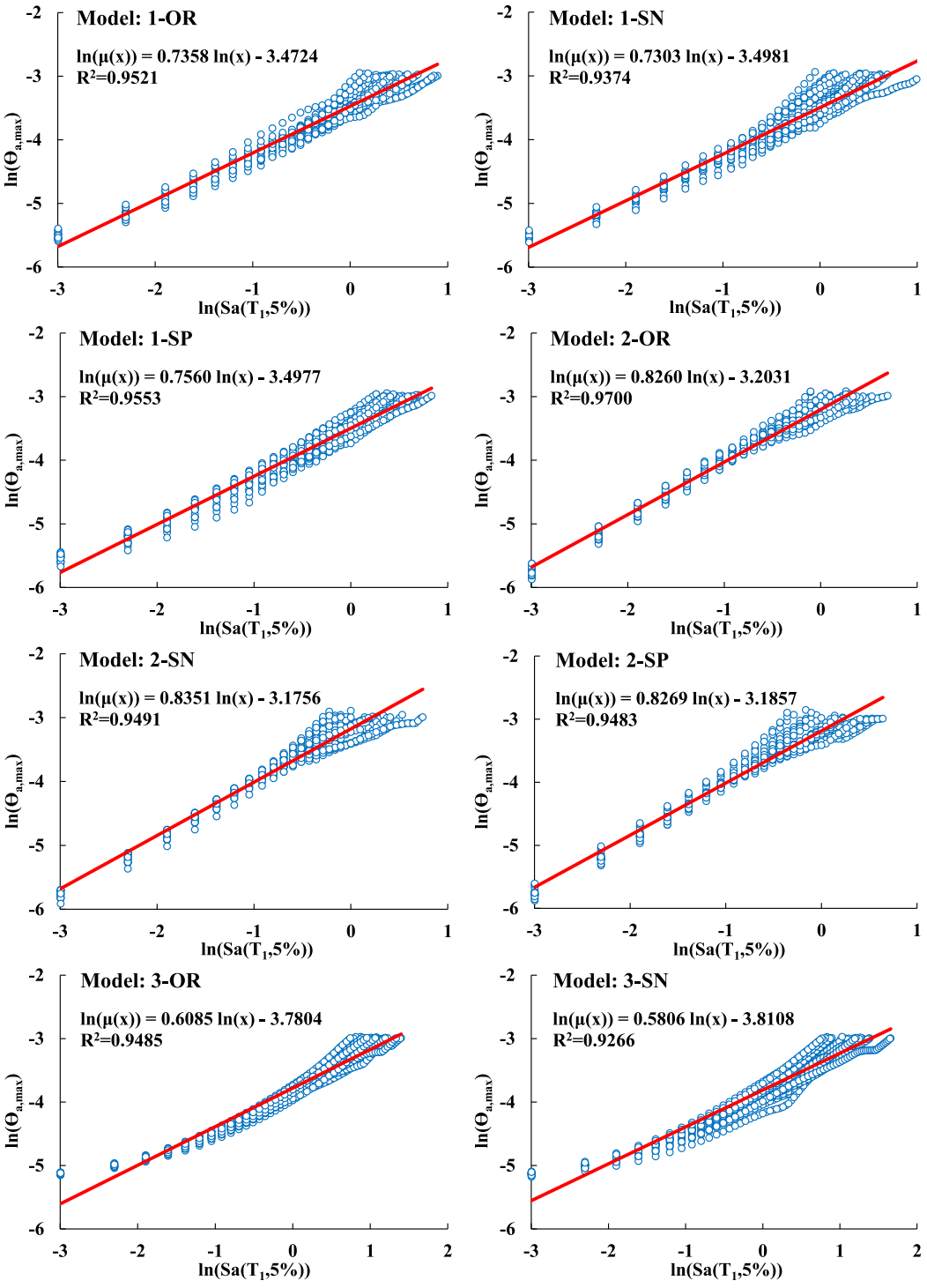

Fig. 9. PSDMs.

analyses under a set of ground motions, the most important step of the validation belongs to this part.

As can be seen in Fig. 5, the dynamic properties and the nonlinear behavior of the structure are almost identical with a slight difference in both pieces of software. As mentioned earlier, SFGs experience a static displacement in the initial state due to gravity loads. After incorporating the ground motion, the absolute maximum displacement for SFGs involves initial static displacement resulting from the gravity loads plus maximum dynamic displacement resulting from the ground motion.

5. Selection of ground motions

The ground motions used in the present study for IDA analysis were selected from the PEER-NGA database [63] with tectonic properties of Class D soil (similar to site soil). They are organized into two main groups. The first group consists of 20 far-fault ground motions that are obtained using Ref. [64] and are presented in Table 4. This set has been selected based on Bin Strategy with large magnitude-long distance (LMLR), so that the moment magnitude (M_W) is 6.5–7 and the closest

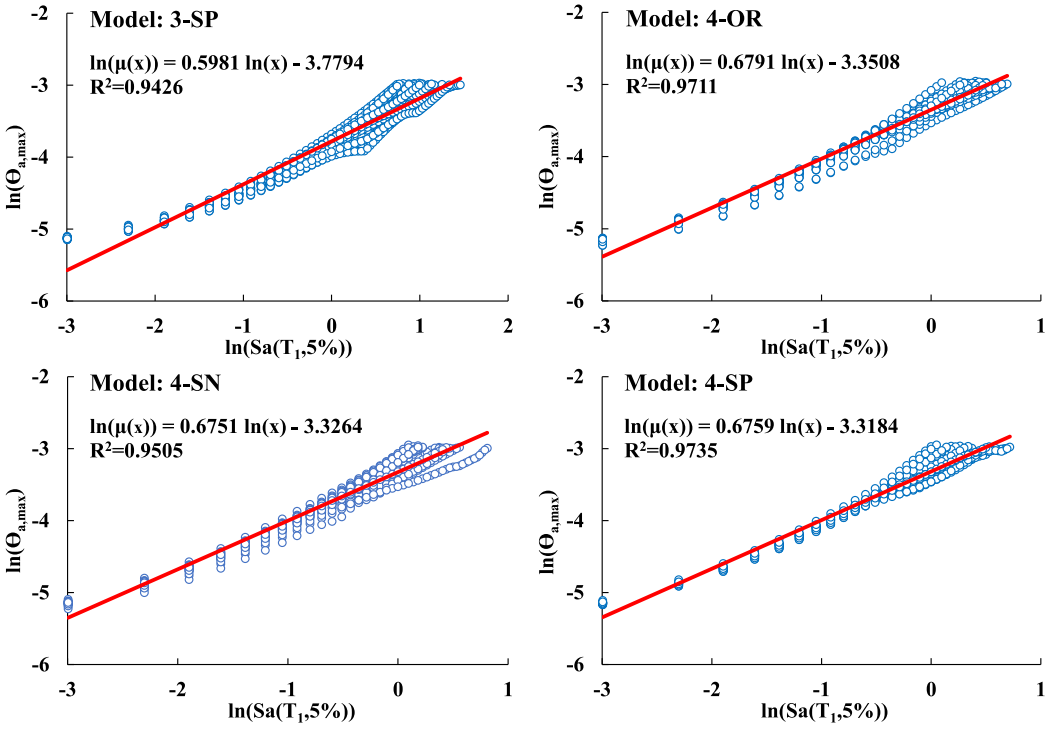

Fig. 9. (*continued*).

Table 6
Estimated unknown parameters of the PSDMs.

Parameters	Model 1			Model 2			Model 3			Model 4		
	OR	SN	SP	OR	SN	SP	OR	SN	SP	OR	SN	SP
a (1.E-02)	3.104	3.025	3.027	4.064	4.177	4.135	2.281	2.213	2.284	3.506	3.592	3.621
b (1.E-01)	7.358	7.303	7.560	8.260	8.351	8.269	6.085	5.806	5.981	6.791	6.751	6.759
σ (1.E-01)	1.431	1.653	1.403	1.223	1.652	1.662	1.286	1.515	1.341	0.995	1.310	0.944

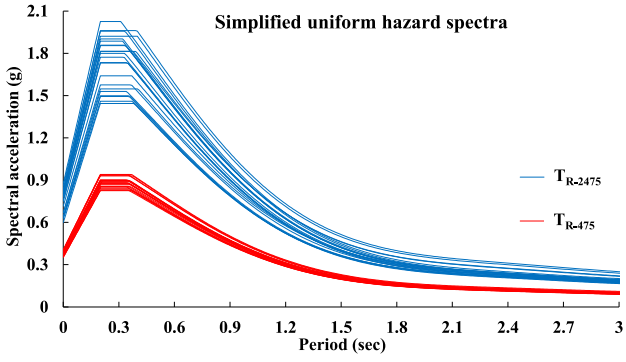

Fig. 10. Simplified uniform hazard spectra with $T_{R\text{-}2475}$ and $T_{R\text{-}475}$ for 22 different regions of Tehran.

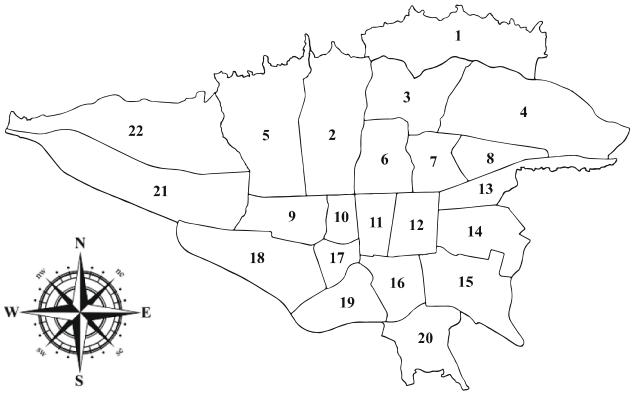

Fig. 11. Regioning map of Tehran.

distance from the recording site to the ruptured area (R_{rup}) is 30–60 km. Additional criteria such as site class, peak values (PGA, PGV and PGD), ground motion duration, strong ground motion duration ($D_{5\text{-}95\%}$), cut-off frequency, and fault mechanism are included in this selection. More information on this set of ground motions and their selection is available in Chapter 3 of Ref. [64]. The second group consists of 20 pairs of near-fault ground motions that are obtained using Ref. [65]. Their M_W is more than 6.5 and R_{rup} is less than 10 km (excluding the Landers earthquake record). These pairs of ground motions are rotated in the strike-normal and strike-parallel directions, where their strike-normal component contains a long-period pulse in the velocity time-history, as determined using the method described by Baker [11], and their characteristics are presented in Table 5. These pulses are expected to occur in some ground motions observed near fault ruptures due to directivity effects, but as noted in the literature, not all pulse-like ground motions are the result of directivity effects and the appearance of pulses is likely caused by effects other than directivity, such as basins effects, surface wave effects or surficial soil effects. For this reason, the simplified

Table 7
Spectral accelerations corresponding to simplified uniform hazard spectra with $T_{R\text{-}475}$ and $T_{R\text{-}2475}$ for 22 different regions of Tehran.

No.	Region name	latitude	Longitude	Model 1		Model 2		Model 3		Model 4	
				Sa_{475}	Sa_{2475}	Sa_{475}	Sa_{2475}	Sa_{475}	Sa_{2475}	Sa_{475}	Sa_{2475}
1	Tajrish	35.79	51.44	0.500	1.090	0.219	0.491	0.723	1.558	0.285	0.629
2	Punak	35.76	51.36	0.490	0.993	0.211	0.443	0.707	1.432	0.275	0.568
3	Vanak	35.76	51.43	0.491	0.991	0.215	0.444	0.713	1.407	0.277	0.568
4	Lavizan	35.73	51.50	0.447	0.785	0.193	0.35	0.643	1.127	0.251	0.447
5	Ekbatan	35.70	51.31	0.471	0.877	0.203	0.384	0.678	1.266	0.263	0.493
6	Arjantin Square	35.72	51.40	0.458	0.843	0.198	0.371	0.666	1.219	0.257	0.475
7	Bahar	35.72	51.43	0.444	0.804	0.190	0.353	0.643	1.151	0.250	0.454
8	Narmak	35.72	51.50	0.443	0.781	0.188	0.344	0.64	1.130	0.246	0.445
9	Mehrabad Airport	35.67	51.30	0.458	0.902	0.196	0.386	0.663	1.312	0.253	0.501
10	Beryanak	35.67	51.36	0.471	0.958	0.204	0.403	0.681	1.386	0.263	0.523
11	Moniriyeh	35.67	51.39	0.472	0.957	0.204	0.401	0.675	1.379	0.264	0.531
12	Baharestan	35.67	51.42	0.461	0.926	0.196	0.385	0.666	1.331	0.254	0.510
13	Tehranno	35.70	51.50	0.438	0.790	0.187	0.342	0.633	1.144	0.245	0.445
14	Chaharsad Dastgah	35.66	51.47	0.452	0.895	0.196	0.379	0.655	1.298	0.254	0.497
15	Afsariyeh	35.63	51.45	0.464	0.961	0.201	0.405	0.668	1.389	0.258	0.532
16	Nazi Abad	35.63	51.41	0.468	1.004	0.200	0.418	0.680	1.447	0.263	0.553
17	Yaft Abad	35.65	51.36	0.464	0.954	0.200	0.401	0.674	1.373	0.260	0.525
18	Ferdows	35.65	51.19	0.434	0.793	0.188	0.348	0.632	1.133	0.243	0.450
19	Nemat Abad	35.61	51.37	0.469	1.025	0.202	0.431	0.676	1.473	0.262	0.559
20	Ray	35.58	51.43	0.438	0.905	0.186	0.375	0.638	1.303	0.242	0.489
21	Tehransar	35.71	51.16	0.462	0.859	0.201	0.387	0.668	1.232	0.259	0.489
22	Chitgar Lake	35.74	51.20	0.495	1.062	0.214	0.478	0.720	1.531	0.280	0.612
Avg.	–	–	–	0.463	0.916	0.200	0.396	0.670	1.319	0.259	0.513

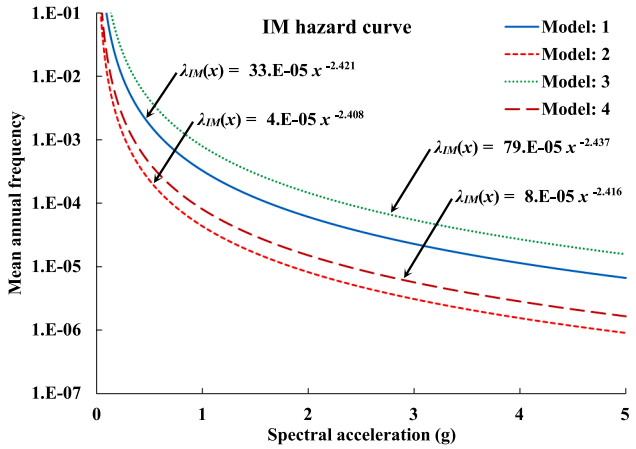

Fig. 12. IM hazard curves.

uniform hazard spectra used in the present study do not explicitly account for directivity-pulse effects. The elastic response spectra (5% damping) of the selected ground motions are generated by Seismosignal software [66] and the average of their elastic response spectra is shown in Fig. 6.

A final summary of the considered sets of ground motions for IDA analysis is given below.

1) OR set (20 ground motions): far-fault ground motions. Since these ground motions do not have impulsive characteristics, they are called ordinary ground motions and are expressed by OR in the present study.
2) SN set (20 ground motions): near-fault pulse-like ground motions. In this set, only the strike-normal component of the ground motions is included, which contains a long-period pulse in the velocity time-history.
3) SP set (20 ground motions): strike-parallel components of the ground motions in the SN set.

6. IDA analysis

IDA analysis includes subjecting a structural model to multiple levels of intensity by scaling the ground motion, so that they can cover the range of linear and nonlinear behaviors as well as the collapse of a structure [67]. IDA technique allows focusing on the frequency content of the ground motion as the whole record is scaled with same intensity level. The primary goal of the IDA technique is to determine the dynamic capacity of the structure against limit states. In the present paper, the 5% damped first-mode spectral acceleration ($Sa(T_1,5\%)$) and the absolute maximum drift angle ($\Theta_{a,max}$) were selected as intensity measure (IM) and damage measure (DM), respectively. The scale factor of records is defined as a multiplication of $Sa(T_1,5\%)$, from a very low level with incremental steps of 0.05 g to a high level where the collapse of the structure occurs, and the $\Theta_{a,max}$ parameter is recorded in each step of the analysis. In the present research, based on FEMA 356, three limit states of immediate occupancy (IO), life safety (LS) and collapse prevention (CP) with the $\Theta_{a,max}$ values of 0.7, 2.5 and 5% were selected, respectively. It should be noted that due to insufficient information of the regulations on the performance-based design of steel gabled frame systems, in the FEMA 356, conventional steel frame systems are used to determine the limit states of the damage measure.

Multi-record IDA curves well demonstrate the structural behavior from the linear region to the collapse of a structure for a set of ground motions selected based on the desired properties. However, multi-record IDA curves indicate a large difference between one ground motion and another. Hence, they should be summarized to reduce data dispersion. A method of summarization is the use of 16%, 50% and 84% percentiles. Summarized IDA curves are also called structural dynamic capacity (tolerable IM value for a structure or IM capacity) curves, which are mainly used to compare structures relative to each other [67]. Multi-record IDA curves and summarized IDA curves (16%, 50% and 84% fractiles) have been determined for the studied SGFs are shown in Fig. 7. Also, for a better comparison between the dynamic capacity of the studied SGFs, the 50% fractile of the IDA curves are given in Fig. 8. As previously described, due to the specific geometrical characteristic of SFGs (sloping beams), gravity loads create an initial negative $\Theta_{a,max}$ in the shoulder and are amplified by the hinge supports, which appears positive in the IDA curves since the $\Theta_{a,max}$ is an absolute value. This can be clearly seen in Figs. 7 and 8.

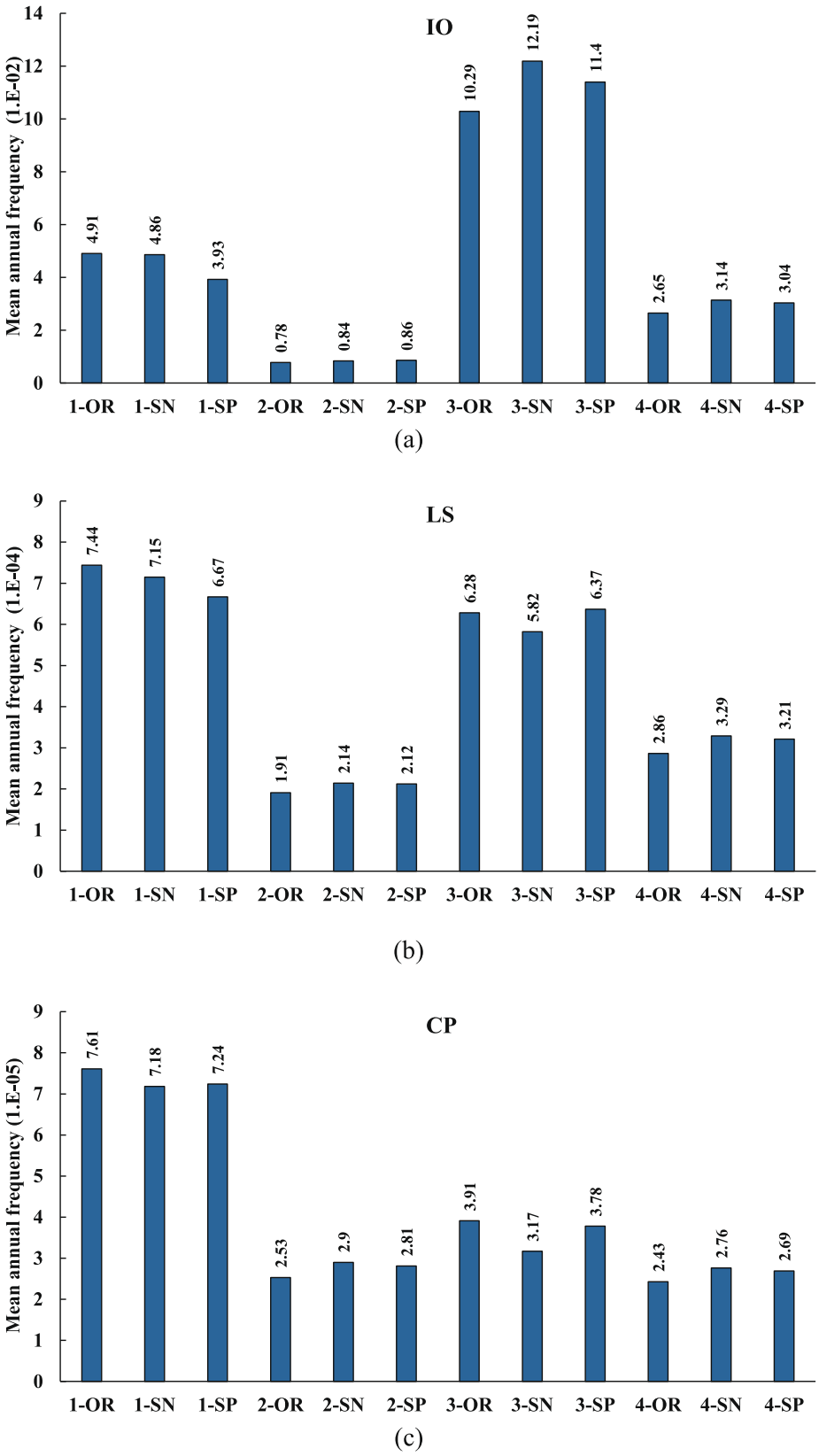

Fig. 13. MAF at (a) IO, (b) LS, and (c) CP limit states.

As can be seen in Fig. 7, in the multi-record IDA curves, the SN ground motions relative to SP and OR raises the changes of stiffness and demand sensitivity in SGFs. Also, the obtained dynamic capacity values from the 50% fractile of the IDA curves, shown in Fig. 8, clearly indicate different seismic behavior in SGFs with various periods under three sets of the OR, SN and SP ground motions. At the CP limit state, the SN ground motions relative to OR reduces the dynamic capacity of Models 1, 2, 3 and 4 by −5, 24, 1 and 17%, respectively; the SP ground motions

Table 8
MAF error between the OR, SN and SP ground motions at the IO, LS and CP limit states.

No.	SN/OR (%)			SP/OR (%)			SN/SP (%)		
	IO	LS	CP	IO	LS	CP	IO	LS	CP
1	−1	−4	−6	−20	−10	−5	24	7	−1
2	8	12	15	10	11	11	−2	1	3
3	18	−7	−19	11	1	−3	7	−9	−16
4	18	15	14	15	12	11	3	2	3

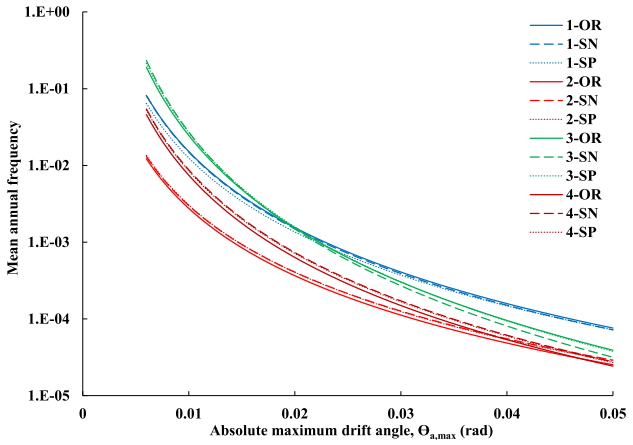

Fig. 14. PSDA curves.

relative to OR by −6, 24, 2 and 10%, respectively; and the SN ground motions relative to SP by 1, 0, −1 and 7%, respectively; so that these amounts at the LS and IO limit states becomes less. Also, under any type of ground motion (OR, SN and SP), Models 1 and 3 have higher dynamic capacity than Models 2 and 4. In addition, due to the initial drift angle due to gravity loads in the models, it has caused them to experience the IO limit state under very low earthquake intensity. This means that the limit state mentioned in the seismic behavior of SGFs cannot be very important.

7. PSDA

7.1. Overview

PSDA is a method to computing the MAF (annual probability) of exceeding a specified demand for a given structure at a designated site. This method integrates the IM hazard curve for the study region, which is computed via probabilistic seismic hazard analysis (PSHA), into the results of IDA analysis of the structure. in fact, this is an application of the total probability theorem, which is also at the foundation of PSHA. Using DM and IM, PSDA is expressed mathematically in Eq. (1) [68]:

$$\lambda_{DM}(y) = \int G_{DM|IM}(y|x).|d\lambda_{IM}(x)| \tag{1}$$

where $\lambda_{DM}(y)$ denotes the MAF of DM exceeding the value y (DM hazard); likewise, $\lambda_{IM}(x)$ is the IM hazard and $d\lambda_{IM}(x)$ is its differential at x. In simplistic terms, $d\lambda_{IM}(x)$ is the annual probability of observing a particular value of IM. The term $G_{DM|IM}(y/x)$, which is usually computed using the results of IDA analysis, denotes the probability of DM exceeding the value y given that IM equals x. It should be noted that the term $G_{DM|IM}(y/x)$ refers to the uncertainty of structural demand at a particular level of IM due to differences among ground motions.

Using the simplifying assumptions detailed below, the PSDA integral for λ_{DM} expressed in Eq. (1) can be solved analytically. The resulting closed-form solution for λ_{DM} is expressed in Eq. (2) [68]:

$$\lambda_{DM}(y) = \lambda_{IM}(IM(y)).CF_{\sigma} \tag{2}$$

where $IM(y)$ denotes the IM corresponding to y, and is expressed in Eq. (3). The correction factor CF_{σ} primarily accounts for the variability in DM given IM according to Eq. (4). The parameters a, b, k, and σ are detailed below.

$$IM(y) = (y/a)^{1/b} \tag{3}$$

$$CF_{\sigma} = exp\left[0.5(k\sigma/b)^2\right] \tag{4}$$

Note that Eq. (2) indicates that $\lambda_{DM}(y)$ can simply be computed as the MAF of exceeding the value of IM that corresponds to y, multiplied by a correction factor that accounts (primarily) for the variability in DM given IM.

The closed-form solution for λ_{DM} expressed in Eq. (2) assumes the following [68]:

- a log–log linear form of the IM hazard curve, as expressed in Eq. (5):

$$\lambda_{IM}(x) = k_0 x^{-k} \tag{5}$$

where k is the log–log slope and k_0 can be thought of as the MAF of exceeding a unit IM.

- a log–log linear functional form for $\mu(x)$ (the median DM given IM), as expressed in Eq. (6):

$$\mu(x) = a.x^b \tag{6}$$

To perform a linear regression analysis, the Eq. (6) is generally rewritten in the form of the logarithms of the μ and IM, as expressed in Eq. (7):

$$ln(\mu(x)) = lna + b.ln(x) \tag{7}$$

where a and b are the regression coefficients of the PSDM.

- a lognormal distribution of DM given IM with the dispersion expressed in Eq. (8):

$$\sigma = \sqrt{\frac{1}{n-2}\sum [ln(DM) - ln(a.x^b)]^2} \tag{8}$$

where n is the number of (DM, IM) data points.

In short, the closed-form solution for λ_{DM} expressed in Eq. (2) has five unknown parameters (i.e., a, b, σ, k and k_0) that must be estimated according to the above assumptions. So first, the unknown parameters a, b and σ are obtained using PSDM. Then, by determining the unknown parameters k and k_0 from the IM hazard curve of the study region, λ_{DM} expressed in Eq. (2) can be solved as a closed form.

7.2. PSDMs

The PSDM which establishes a linear regression of μ-IM, is obtained using the results of IDA analysis and the power law function [69]. This linear regression model is used to determine the slope (b), intercept (a), and dispersion (σ) of the μ-IM relationship. As described in Section 7-1, in the present study, using the linear regression model expressed in Eq. (7), the regression coefficients of the PSDMs for the studied SGFs are estimated and then using Eq. (8) the dispersion of each model is computed. Fig. 9 shows the PSDMs for the studied SGFs. Each figure also depicts the corresponding linear regression equation and R^2 value. Also, the unknown parameters of the PSDMs (a, b and σ), which are the main core in seismic demand estimation, are presented in Table 4. These models can form a basis for the estimation of the probabilistic seismic demand and performance-based design of such structures.

From Fig. 9, it is evident that all the PSDMs have a R^2 value greater

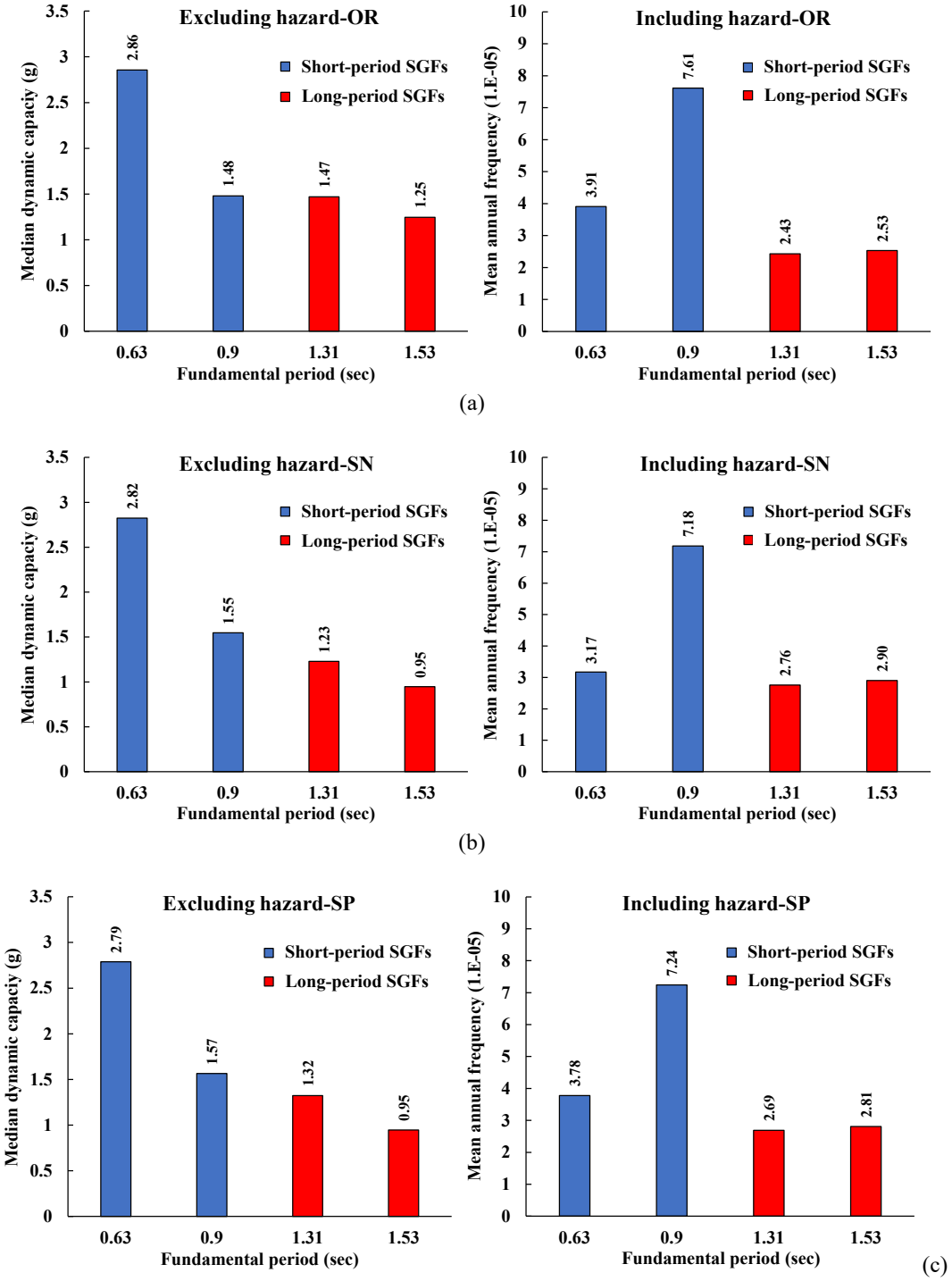

Fig. 15. Comparison of median dynamic capacity (excluding hazard) and MAF (including hazard) at CP limit state for (a) OR, (b) SN, (c) SP ground motions.

that 0.92 which indicates a very strong correlation between the considered DM and IM. As can be seen in Table 6, on average in all SGFs, the dispersion of the PSDMs for the OR, SN and SP ground motions are 0.123, 0.153 and 0.134, respectively. Moreover, under any type of ground motion (OR, SN and SP), the slope of the PSDMs in models 1 and 2 are greater than models 3 and 4 as well as their intercept in models 2 and 4 are greater than models 1 and 3.

7.3. IM hazard curves

To solve the closed form λ_{DM} expressed in Eq. (2), in addition to having the unknown parameters of the PSDMs, it is necessary to estimate the unknown parameters k and k_0 from the IM hazard curve. However, in order to calculate the unknown parameters k and k_0 from the IM hazard curve, PSHA for the study region is required. By determining the simplified uniform hazard spectra with 475-year and 2475-year return periods ($T_{R\text{-}475}$ and $T_{R\text{-}2475}$, respectively) for the study region, the estimation of the unknown parameters k and k_0 from the IM hazard curve is easily achievable, which is discussed in detail below.

As described in Section 7-1, in the present study, using Eq. (7), the IM hazard curves for the studied SGFs are estimated. Nevertheless, the unknown parameters k and k0 must be calculated to determine the IM

hazard curve. To this end, the following steps need to be taken. (a) The simplified uniform hazard spectra with $T_{R\text{-}475}$ and $T_{R\text{-}2475}$ for Class D soil are obtained using Ref. [70] for 22 different regions of Tehran (see Fig. 10). The regioning map of Tehran is shown in Fig. 11. Also, latitude, longitude and the name of each region are presented in Table 7. (b) The spectral accelerations corresponding to the fundamental period of the studied SGFs are determined using the simplified uniform hazard spectra with $T_{R\text{-}475}$ and $T_{R\text{-}2475}$ (Sa_{475} and Sa_{2475}, respectively) for 22 different regions of Tehran (see Table 7). (c) The average of the mentioned spectral accelerations for the studied SGFs are estimated, which are expressed as $Sa_{475,avg}$ and $Sa_{2475,avg}$, respectively (see Table 7). (d) λ_{IM} is considered equal to the inverse of $T_{R\text{-}475}$ and $T_{R\text{-}2475}$ and IM is equal to the $Sa_{475,avg}$ and $Sa_{2475,avg}$. Keeping the above in mind, Eq. (5) can be rewritten into the following form:

$$\begin{cases} \dfrac{1}{T_{R\,-\,475}} = k_0 \left(Sa_{475,avg}\right)^{-k} \\ \dfrac{1}{T_{R\,-\,2475}} = k_0 \left(Sa_{2475,avg}\right)^{-k} \end{cases} \tag{9}$$

By solving the two-equation and two-unknown system in Eq. (9), the unknown parameters k and k_0 are calculated. Then, by putting the values of k and k_0 in Eq. (5), the IM hazard curves for the studied SGFs are obtained (see Fig. 12).

7.4. MAF of the limit states

Using the unknown parameters of the PSDMs as well as the IM hazard curves given in Sections 7.2 and 7.3, λ_{DM} expressed in Eq. (2) for the IO, LS and CP limit states were solved as a closed form, the results of which are shown in Fig. 13. Also in Table 8, MAF error between the OR, SN and SP ground motions at the IO, LS and CP limit states is presented. These values can be used as a criterion for measuring the reliability of the structures under study in comparison with other structural systems or they can be employed in the codes related to the design of such structures.

Fig. 13 and Table 8 clearly shows the difference between the MAF values for SGFs with various periods under three sets of the OR, SN and SP ground motions. On average at all limit states, the SN ground motions relative to OR increases the MAF of Models 1, 2, 3 and 4 by −4, 12, −3 and 16%, respectively; for the SP ground motions relative to OR by −12, 11, 3 and 13%, respectively; and for the SN ground motions relative to SP by 10, 1, −6 and 3%, respectively. Also, the rate of change of MAF error between the OR, SN and SP ground motions at the IO, LS and CP limit states in Models 1 and 3 are higher than Models 2 and 4.

7.5. PSDA curves

The output of the PSDA is the curves that estimate the MAF for different values of DM, each of which can be considered as a limit state. Hence, λ_{DM} expressed in Eq. (2) for different values of DM were solved as a closed form, the results of which are shown in Fig. 14. These curves can be used in the performance-based design for such structures to determine the design earthquakes with return periods commensurate with a given DM.

As can be seen in Fig. 14, on average in all $\Theta_{a,max}$'s, near-fault ground motions (especially pulse-like ones) increase the MAF in Models 2 and 4 compared to far-fault ground motions and slightly reduce the MAF in Models 1 and 3. Moreover, the rate of change of MAF error between the OR, SN and SP ground motions in all $\Theta_{a,max}$'s in Models 1 and 3 are higher than Models 2 and 4. Also, under any type of ground motion (OR, SN and SP), the rate of change of MAF in all $\Theta_{a,max}$'s in Models 3 and 4 are higher than Models 1 and 2. However, in all $\Theta_{a,max}$'s, under any type of ground motion (OR, SN and SP), Models 1 and 3 have higher MAF than Models 2 and 4, while according to the observations of Section 6, the median dynamic capacity of models 1 and 3 was higher than models 2 and 4. For a better comparison of the two outputs at the CP limit state, the median dynamic capacity (excluding hazard) and the MAF (including hazard) for the studied models under OR, SN and SP ground motions are shown in Fig. 15.

8. Conclusion

In this study, IDA analysis was performed on four SGFs with the bays of 20 m and 60 m and heights of 6 m and 12 m using the OR, SN and SP ground motions for the first time. The results were presented in the form of multi-record IDA curves, summarized IDA curves, PSDMs and PSDA curves. Some of the main findings as the contributions of the present research are as follows:

- According to the multi-record IDA curves, the SN ground motions relative to SP and OR raised the changes of stiffness and demand sensitivity in SGFs.
- According to the 50% fractile of the IDA curves, near-fault ground motions (especially pulse-like ones) reduced the dynamic capacity in long-period SGFs compared to far-fault ground motions and slightly increased the dynamic capacity in short-period SGFs, and these amounts were more significant at the CP limit state than LS and IO. At the CP limit state, for the SN ground motions relative to OR, the largest reductions the dynamic capacity were related to Models 2 and 4 (long-period SGFs) with 24 and 17% and the smallest were related to Models 1 and 3 (short-period SGFs) with −5 and 1%, respectively; and for the SP ground motions relative to OR, the largest reductions the dynamic capacity were belonged to Models 2 and 4 (long-period SGFs) with 24 and 10% and the smallest were belonged to Models 1 and 3 (short-period SGFs) with −6 and 2%, respectively. However, the dynamic capacity of SGFs under near-fault ground motions (SN and SP) relative to each other did not depend on their fundamental period, and on average in all models, at the CP limit state, the SN ground motions relative to SP reduced the dynamic capacity by 7%. Also, under any type of ground motion (OR, SN and SP), short period SGFs had higher dynamic capacity than long period SGFs.
- According to the PSDMs, the SN ground motions relative to SP and OR enhanced the data dispersion and uncertainty in SGFs, and on average in all models, the dispersion of the PSDMs for the SN, SP and OR ground motions were 0.153, 0.134 and 0.123, respectively. Also, the use of $Sa(T_1,5\%)$ and $\Theta_{a,max}$ as IM and DM, respectively, led to very accurate PSDMs in SGFs.
- According to the MAF of the limit states, on average at all limit states, near-fault ground motions (especially pulse-like ones) increased the MAF in long-period SGFs compared to far-fault ground motions and slightly reduced the MAF in short-period SGFs. For the SN ground motions relative to OR, the highest increases the MAF were related to Models 2 and 4 (long-period SGFs) with 12 and 16% and the lowest were related to Models 1 and 3 (short-period SGFs) with −4 and −3%, respectively; and for the SP ground motions relative to OR, the highest increases the MAF were belonged to Models 2 and 4 (long-period SGFs) with 11 and 13% and the lowest were belonged to Models 1 and 3 (short-period SGFs) with −12 and 3%, respectively. However, the MAF of SGFs under near-fault ground motions (SN and SP) relative to each other did not depend on their fundamental period, and on average in all models, the SN ground motions relative to SP increased the MAF by 8%.
- According to the PSDA curves, on average in all $\Theta_{a,max}$'s, near-fault ground motions (especially pulse-like ones) increased the MAF in long-period SGFs compared to far-fault ground motions and slightly reduced the MAF in short-period SGFs. However, in all $\Theta_{a,max}$'s, under any type of ground motion (OR, SN and SP), short-period SGFs had higher MAF than long-period SGFs.
- According to the outcomes of the 50% fractile of the IDA curves and the PSDA curves, the combination of hazard curve of the study region with the results of IDA analysis of the structure was of great

importance in evaluating the seismic behavior of SGFs. Without incorporating the IM hazard curve, short period SGFs had higher dynamic capacity than long period SGFs, however, after integrating the IM hazard curve with the results of IDA analysis, the outcomes were completely reversed so that short-period SGFs had higher MAF than long-period SGFs. This is due to the fact that in the IM hazard curves, the MAF values decrease with increasing the fundamental period of SGFs.

- The fundamental period of SGFs was an important factor in the amount of damage caused by near-fault ground motions (especially pulse-like ones) relative to far-fault ground motions and did not dependent on their geometric dimensions, which increased the damage in long-period SGFs as well as slightly reduced the damage in short-period SGFs. However, the fundamental period of SGFs was not a significant factor in the amount of damage caused by near-fault ground motions (SN and SP) relative to each other.

In general, the outcomes showed the importance of near-fault ground motions (especially pulse-like ones) on the seismic behavior of long-period SGFs, so that compared to far-fault ground motions produced significant changes on their seismic behavior. On the other hand, the near-fault effects have no significant role on the seismic behavior of short-period SGFs, so that far-fault ground motions partially lead to more damage compared to near-fault ground motions. However, under any type of ground motion, short-period SGFs are more vulnerable than long-period SGFs. Finally, it was observed that the combination of hazard curve of the study region with the results of IDA analysis of the structure is of great importance in evaluating the seismic behavior of SGFs. Disregarding the IM hazard curve in the study of SGFs can lead to a meaningful deviation of the outcomes from the actual results. Therefore, it is recommended that seismic design codes take a more specific look at near-fault ground motions (especially pulse-like ones) in long-period SGFs, while the near-fault effects can be ignored in short period SGFs. Also, under any type of ground motion, in high-seismicity regions (such as Tehran), short-period SGFs should be prioritized for retrofitting than long-period SGFs. It should be noted that the PSDA results are presented specifically for the city of Tehran and these results are valid for the areas with high seismicity such as Tehran. Finally, the combination of hazard curve of the study region with the results of IDA analysis of the structure in evaluating the seismic behavior of SGFs should be emphasized.

Declaration of Competing Interest

The authors declare that they have no known competing financial interests or personal relationships that could have appeared to influence the work reported in this paper.

References

[1] Wang GQ, Zhou XY, Zhang PZ, et al. Characteristics of amplitude and duration for near-fault strong ground motion from the1999 Chi-Chi, Taiwan earthquake. Soil Dyn Earthquake Eng 2002;22(1):73–96. https://doi.org/10.1016/S0267-7261(01)00047-1.

[2] Mavroeidis GP, Papageorgiou AS. A mathematical representation of near-fault ground motions. Seismol Soc Am 2003;93(3):1099–131. https://doi.org/10.1785/0120020100.

[3] Yang D, Wang W. Nonlocal period parameters of frequency content characterization for near-fault ground motions. Earthquake Eng Struct Dyn 2012;41(13):1793–811. https://doi.org/10.1002/eqe.2157.

[4] Kalkan E, Kunnath SK. Effects of fling step and forward directivity on seismic response of buildings. Earthquake Spectra 2006;22(2):367–90. https://doi.org/10.1193/1.2192560.

[5] Somerville PG, Smith NF, Graves RW, et al. Modification of empirical strong ground motion attenuation relations to include the amplitude and duration effects of rupture directivity. Seismol Res Lett 1997;68(1):199–222. https://doi.org/10.1785/gssrl.68.1.199.

[6] Somerville PG. Magnitude scaling of the near fault rupture directivity pulse. Phys Earth Planet Inter 2003;137:201–12. https://doi.org/10.1016/S0031-9201(03)00015-3.

[7] Park J, Fenves GL, Stojadinovic B. Spatial distribution of response of multi-story structures for simulated ground motions. In: 13th World Conference on Earthquake Engineering. Canada; 2004.

[8] Bray JD, Rodriguez-Marek A. Characterization of forward-directivity ground motions the near-fault region. Soil Dyn Earthquake Eng 2004;24(11):815–28. https://doi.org/10.1016/j.soildyn.2004.05.001.

[9] Yang D, Zhou J. A stochastic model and synthesis for near-fault impulsive ground motions. Earthquake Eng Struct Dyn 2015;44(2):243–64. https://doi.org/10.1002/eqe.2468.

[10] Spudich P, Chiou BSJ. Directivity in NGA earthquake ground motions: analysis using isochrone theory. Earthquake Spectra 2008;24(1):279–98. https://doi.org/10.1193/1.2928225.

[11] Baker JW. Quantitative classification of near-fault ground motions using wavelet analysis. Bull Seismol Soc Am 2007;97(5):1486–501. https://doi.org/10.1785/0120060255.

[12] Champion C, Liel A. The effect of near-fault directivity on building seismic collapse risk. Earthquake Eng Struct Dyn 2012;41(10):1391–409. https://doi.org/10.1002/eqe.1188.

[13] Shahi SK, Baker JW. An efficient algorithm to identify strong-velocity pulses in multicomponent ground motions. Bull Seismol Soc Am 2014;104(5):2456–66. https://doi.org/10.1785/0120130191.

[14] Bradley BA. Period dependence of response spectrum damping modification factors due to source-and site-specific effects. Earthquake Spectra 2015;31(2):745–59. https://doi.org/10.1193/070213EQS189M.

[15] Moustafa A, Takewaki I. Deterministic and probabilistic representation of nearfield pulse-like ground motion. Soil Dyn Earthquake Eng 2010;30(5):412–22. https://doi.org/10.1016/j.soildyn.2009.12.013.

[16] Alonso-Rodríguez A, Miranda E. Assessment of building behavior under near-fault pulse-like ground motions through simplified models. Soil Dyn Earthquake Eng 2015;79:47–58. https://doi.org/10.1016/j.soildyn.2015.08.009.

[17] Chang ZW, Sun XD, Zhai CH, Zhao JX, Xie LL. An improved energy-based approach for selecting pulse-like ground motions. Earthquake Eng Struct Dyn 2016;45:2405–11. https://doi.org/10.1002/eqe.2758.

[18] Dabaghi M, Der Kiureghian A. Stochastic model for simulation of near-fault ground motions. Earthquake Eng Struct Dyn 2017;46(6):963–84. https://doi.org/10.1002/eqe.2839.

[19] Yang D, Guo G, Liu Y, et al. Dimensional response analysis of bilinear SDOF systems under near-fault ground motions with intrinsic length scale. Soil Dyn Earthquake Eng 2019;116:397–408. https://doi.org/10.1016/j.soildyn.2018.10.034.

[20] Zou D, Han H, Ling H, et al. An approach for the real-time slip deformation coupled with strain softening of a high rockfill dam subjected to pulse-like ground motions. Soil Dyn Earthquake Eng 2019;117:30–46. https://doi.org/10.1016/j.soildyn.2018.10.044.

[21] Wu Q, Li DQ, Liu Y, et al. Seismic performance of earth dams founded on liquefiable soil layer subjected to near-fault pulse-like ground motions. Soil Dyn Earthquake Eng 2021;143:106623. https://doi.org/10.1016/j.soildyn.2021.106623.

[22] Bayraktar A, Altunisik AC, Sevim B, et al. Near-fault ground motions effects on the nonlinear response of dam-reservoir-foundation systems. Struct Eng Mech 2008;28(4):411–42. https://doi.org/10.12989/sem.2008.28.4.411.

[23] Bayraktar A, Turker T, Akkose M, et al. The effect of reservoir length on seismic performance of gravity dams to near- and far-fault ground motions. Nat Hazards 2010;52:257–75. https://doi.org/10.1007/s11069-009-9368-1.

[24] Zou D, Han H, Liu J, et al. Seismic failure analysis for a high concrete face rockfill dam subjected to near-fault pulse-like ground motions. Soil Dyn Earthquake Eng 2017;98:235–43. https://doi.org/10.1016/j.soildyn.2017.03.031.

[25] Beiraghi H, Kheyroddin A, Kafi MA. Forward directivity near-fault and far-fault ground motion effects on the behavior of reinforced concrete wall tall buildings with one and more plastic hinges. Soil Dyn Earthquake Eng 2016;25(11):519–39. https://doi.org/10.1002/tal.1270.

[26] Li C, Kunnath S, Zuo Z, et al. Effects of early-arriving pulse-like ground motions on seismic demands in RC frame structures. Soil Dyn Earthquake Eng 2020;130:105997. https://doi.org/10.1016/j.soildyn.2019.105997.

[27] Mohammadi MH, Massumi A, Meshkat-Dini A. Performance of RC moment frames with fixed and hinged supports under near-fault ground motions. Earthquakes Struct 2017;13(1):89–101. https://doi.org/10.12989/eas.2017.13.1.089.

[28] Ji K, Ren Y, Wen R, et al. Near-field velocity pulse-like ground motions on February 6, 2018 MW6.4 Hualien, Taiwan earthquake and structural damage implications. Soil Dyn Earthquake Eng 2019;126(105784). https://doi.org/10.1016/j.soildyn.2019.105784.

[29] Mazza F, Vulcano A. Effects of near-fault ground motions on the nonlinear dynamic response of base-isolated r.c. framed buildings. Earthquake Eng Struct Dyn 2012;41(2):211–32. https://doi.org/10.1002/eqe.1126.

[30] Bhagat S, Wijeyewickrema AC, Subedi N. Influence of near-fault ground motion with fling-step and forward-directivity characteristics on seismic response of base-isolated buildings. J Earthquake Eng 2018;22:1–20. https://doi.org/10.1080/13632469.2018.1520759.

[31] Mazza F. Seismic demand of base-isolated irregular structures subjected to pulse-type earthquakes. Soil Dyn Earthquake Eng 2018;108:111–29. https://doi.org/10.1016/j.soildyn.2017.11.030.

[32] Chen X, Liu Y, Zhou B, et al. Seismic response analysis of intake tower structure under near-fault ground motions with forward-directivity and fling-step effects. Soil Dyn Earthquake Eng 2020;132(106098). https://doi.org/10.1016/j.soildyn.2020.106098.

[33] Li N, Li Q, Ren T. Dynamic response analysis of Zipingpu intake tower under Wenchuan earthquake action. Chinese J Underground Space Eng 2014;10(5):1127–34.
[34] Li S, Zhang F, Wang JQ, et al. Effects of near-fault motions and artificial pulse-type ground motions on super-span cable-stayed bridge systems. J Bridge Eng 2017;22(3):04016128. https://doi.org/10.1061/(ASCE)BE.1943-5592.0001008.
[35] Xin L, Li X, Zhang Z, et al. Seismic behavior of long-span concrete-filled steel tubular arch bridge subjected to near-fault fling-step motions. Eng Struct 2019;180:148–59. https://doi.org/10.1016/j.engstruct.2018.11.006.
[36] Kabir MR, Billah AHMM, Alam MS. Seismic fragility assessment of a multi-span RC bridge in Bangladesh considering near-fault, far-field and long duration ground motions. Structures 2019;19:333–48. https://doi.org/10.1016/j.istruc.2019.01.021.
[37] Konagai K, Yoshimi M, Meguro K, et al. In: Strain induced in cracked utility poles and damage to dwellings from the Dec. 26, 2003 Bam earthquake. Bulletin of Earthquake Research Institute, University of Tokyo; 2004. p. 59–67.
[38] Mashayekhi AH, Gerami M, Siahpolo N. Assessment of higher modes effects on steel moment resisting structures under near-fault earthquakes with forward directivity effect along strike-parallel and strike-normal components. Int J Steel Struct 2019;19(5):1543–59. https://doi.org/10.1007/s13296-019-00229-z.
[39] Lee GC, Ketter RL, Morrell ML. Design of tapered members. Welding Research Council Bulletin, No. 173, New York, USA; 1972.
[40] Lee GC, Morrell ML. Application of AISC design provisions for tapered members. Eng J 1975;12(1):1–13.
[41] Lee GC, Chen YC, Hsu TL. Allowable axial stress of restrained multi-segment, tapered roof girders. Welding Research Council Bulletin, No. 248, New York, USA; 1979.
[42] Lee GC, Hsu TL. Tapered columns with unequal flanges. Welding Research Council Bulletin, No. 272, New York, USA; 1981.
[43] Forest R, Murray TM. Rigid Frame Studies. Report No. FSEL/STAR 82–01. Norman, USA: School of Civil Engineering and Environmental Science, University of Oklahoma; 1982.
[44] Shiomi H, Kurata M. Strength formula for tapered beam-columns. J Struct Eng 1984;110(7):1630–43. https://doi.org/10.1061/(ASCE)0733-9445(1984)110:7(1630).
[45] Ashakul A, Murray TM. LRFD versus ASD frame design study. Report No. CE/VPI-ST 02/02. Blacksburg, USA: Department of Civil and Environmental Engineering, Virginia Polytechnic Institute and State University; 2002.
[46] Hwang JS, Chang KC, Lee GC. Seismic behavior of gable frame consisting of tapered members. J Struct Eng 1991;117(3):808–21. https://doi.org/10.1061/(ASCE)0733-9445(1991)117:3(808).
[47] Hong JK, Uang CM. Cyclic testing of a metal building moment frame system with web-tapered members. J Constr Steel Res 2012;70:248–55. https://doi.org/10.1016/j.jcsr.2011.09.005.
[48] Su M, Wang H, Wang Z, et al. Shaking table tests on steel portal frames consisting of non-compact tapered members. J Constr Steel Res 2017;128:473–82. https://doi.org/10.1016/j.jcsr.2016.09.009.
[49] Jalayer F. Direct probabilistic seismic analysis: implementing non-linear dynamic assessments. California, USA: Stanford University; 2003.
[50] Ruiz-Garcia J, Miranda E. Performance-based assessment of existing structures accounting for residual displacements. California, USA: Stanford University; 2005.
[51] Ruiz-Garcia J, Miranda E. Probabilistic estimation of residual drift demands for seismic assessment of multi-story framed buildings. Eng Struct 2010;32(1):11–20. https://doi.org/10.1016/j.engstruct.2009.08.010.
[52] Baker JW, Cornell CA. A vector-valued ground motion intensity measure consisting of spectral acceleration and epsilon. Earthquake Eng Struct Dyn 2005;34(10):1193–217. https://doi.org/10.1002/eqe.474.
[53] NEHRP. Recommended provisions for seismic regulations for new buildings. Building Seismic Safety Council. Washington DC, USA; 2000.
[54] ASCE/SEI 7–10. Minimum design loads and associated criteria for buildings and other structures. Reston, Virginia, USA: American Society of Civil Engineers in partnership with Structural Engineering Institute; 2010.
[55] AISC 360–10. Specification for structural steel buildings. Chicago, Illinois, USA: American Institute of Steel Construction; 2010.
[56] AISC 341–10. Seismic provisions for structural steel buildings. Chicago, Illinois, USA: American Institute of Steel Construction; 2010.
[57] OpenSees. Open System for Earthquake Engineering Simulation. Berkeley, California, USA: Pacific Earthquake Engineering Research Center. University of California; 2018.
[58] Chopra AK. Dynamics of structures: theory and applications to earthquake engineering. Englewood Cliffs, New Jersey, USA: Prentice-Hall; 2007.
[59] Watwood VB. Gable frame design considerations. J Struct Eng 1985;111(7):1543–58. https://doi.org/10.1061/(ASCE)0733-9445(1985)111:7(1543).
[60] Liu SW, Bai R, Chan SL. Second-order analysis of non-prismatic steel members by tapered beam-column elements. Structures 2016;6:108–18. https://doi.org/10.1016/j.istruc.2016.02.006.
[61] SAP2000. Version 19.2.2. Analysis Reference Manual. Berkeley, California, USA: Computers and Structures Inc. University of California; 2018.
[62] FEMA 356. Prestandard and commentary for the seismic rehabilitation of buildings. Washington, DC, USA: Federal Emergency Management Agency; 2000.
[63] PEER-NGA Database, Pacific Earthquake Engineering Research Center, University of California, Berkeley, California, USA; 2006. <https://www.peer.berkeley.edu/nga/>.
[64] Medina RA, Krawinkler H. Seismic demands for nondeteriorating frame structures and their dependence on ground motions. Report No. 144. California, USA: Stanford University; 2003.
[65] Baker JW, Lin T, Shahi SK, et al. New ground motion selection procedures and selected motions for the PEER transportation. PEER Report 2011/03. Berkeley, California, USA: University of California; 2011.
[66] Antoniou S, Pinho R, Bianchi F. SeismoSignal. Version 3.2.0; 2008.
[67] Vamvatsikos D, Cornell CA. Applied incremental dynamic analysis. Earthquake Spectra 2004;20(2):523–53. https://doi.org/10.1193/1.1737737.
[68] Luco N. Probabilistic seismic demand analysis, SMRF connection fractures, and near-source effects. Ph.D. dissertation. California, USA: Stanford University; 2002.
[69] Cornell CA, Jalayer F, Hamburger RO, et al. Probabilistic basis for 2000 SAC federal emergency management agency steel moment frame guidelines. J Struct Eng 2002;128(4):526–32. https://doi.org/10.1061/(ASCE)0733-9445(2002)128:4(526).
[70] Gholipoor Y, Bozorgnia Y, Rahnama M, et al. Probabilistic seismic hazard analysis phase I Tehran regions final report. Tehran, Iran: Engineering Optimization Research Group. University of Tehran; 2009.